This article has been accepted for publication in IEEE Open Journal of Power Electronics. This is the author's version which has not been fully edited and content may change prior to final publication. Citation information: DOI 10.1109/OJPEL.2023.3239414

An Expanded Lyapunov-Function Based Control Strategy for Cascaded H-Bridge Multilevel Active Front-End Converters

Garry Jean-Pierre*, Necmi Altin †, *Senior Member, IEEE* Ahmad El Shafei *, Adel Nasiri ‡, *Fellow, IEEE*
*Center for Sustainability Electrical Energy System, University of Wisconsin Milwaukee (UWM), Milwaukee, USA
†Electrical-Electronics Engineering Department, Faculty of Technology, Gazi University, Ankara, Turkey
‡ Electrical Engineering Department, College of Engineering and Computing, University of South Carolina (USC), USA

***Abstract*—Cascaded H-bridge multilevel (CHBML) active front-end (AFE) converters exhibit some enticing benefits, comprising high adaptability for numerous applications, such as tractions, solid-state transformers, electric vehicle charging stations, and medium and high power electric drives. Yet, when the CHBML-AFE is operating under an unbalanced load condition, it is crucial to utilize an advanced control technique to maintain system stability. In this research, a Lyapunov Function (LF)-based control approach is utilized for regulating a single-phase CHBML-AFE with LCL filter to achieve global asymptotic stability. A capacitor voltage feedback is introduced and added to the traditional LF-based control strategy to reduce the resonance of the LCL filter. Furthermore, the proportional-resonant (PR) control procedure is utilized to derive the grid current reference, offering improvement to the robustness of the current control design. A balanced DC voltage control method is also employed to suppress the unbalanced DC voltage conditions among CHBML-AFE cells. In addition, the transfer function of the reference grid current and the actual grid current is evaluated for the CHBML-AFE with LCL filter parameters and their eventual variations in the employed control technique. The effectiveness of this control strategy is validated utilizing simulation and experimental studies.**

***Index Terms*—Cascaded H-bridge, current control, LCL filter, Lyapunov Function, proportional-resonant, voltage balancing**

I. Introduction

A highly efficient and power dense power converter is vital for many applications, including aerospace, navy, and renewable systems. Therefore, multilevel converters, which have several advantages over the conventional two-level converters, have gained increasing interest. Among them, the CHBML converter has been identified as the most compelling multilevel configuration due to its characteristics, including modularity, high reliability, high power quality, the need for fewer components, and the decreased cost compared to its counterparts with the same voltage level, especially for medium voltage applications [1], [2]. When constructed as an AC-DC converter, having numerous DC-link voltages for different load ratings is advantageous. Therefore, the CHBML-AFE structure is an attractive solution for solid-state transformer, traction, and medium and high power motor drive applications [3], [4].

Generally, L and LCL are the two most common types of filters used in AFE applications to reduce the converter current harmonics. The LCL filter is the most extensively used configuration, due to its capability to provide good attenuation, low current ripple, and enable operation at lower switching frequency. However, it introduces two extra complex-conjugate poles, which can potentially cause closed-loop instability in the system, resulting in the need for resonant damping for better performance. Therefore, a suitable control technique design can be cumbersome. Many strategies have been used to mitigate the damping issue. The use of dissipative resistors in series or in parallel with the LCL filter components for passive damping was investigated in [5]. Although, the passive damping is a straightforward and cost effective solution, it results in additional power loss and the deterioration of the harmonic attenuation performance of the LCL filter. Therefore, active damping methods have been proposed. The virtual resistor based active damping theory was studied in [6] and [7]. Superior attenuation and damping can be obtained with active damping methods, however the control complexity is increased. The method proposed in [8] is considered for designing the LCL filter because it offers a systematic design methodology that meets industry standards requirements and limits THD to a specific value.

The CHBML-AFE converter controller generally contains an output DC bus voltage control, a grid voltage synchronization entity, and a utility current regulator. Various control methods to address output DC bus voltage control and utility current regulation in CHBML-AFEs have been presented in literature. The deadbeat current regulator was implemented in [2] to reduce the current error at each consecutive sampling period. Even though this method offers a fast transient response, it is sensitive to variation in system parameters [9], [10]. A method based on the finite model predictive control was presented in [11] to reduce computational complexity and improve the steady-state performance of the current. In order to regulate both the voltage and current of the system, cascaded PI controllers were utilized in [12]. Hysteresis current control strategies were proposed and studied in [13] and [14] to reduce

This work is licensed under a Creative Commons Attribution 4.0 License. For more information, see https://creativecommons.org/licenses/by/4.0/

This article has been accepted for publication in IEEE Open Journal of Power Electronics. This is the author's version which has not been fully edited and content may change prior to final publication. Citation information: DOI 10.1109/OJPEL.2023.3239414

the current harmonics of the grid. Although this method is simple, it has drawbacks, such as high current harmonics and variable switching frequency. The PR current regulator was analyzed in [15] for tracking sinusoidal signal. The predictive current regulator was implemented in [16] and [17] to decrease switching frequency. A harmonic current rejection PWM regulator method was used in [18] to decrease the harmonics.

The sliding mode control (SMC) method has been successfully employed in the control of power converters due to these benefits: improved performance against parameter variations and external disturbances, rapid dynamic transient response, and simplicity of implementation [19], [20]. The SMC was also used in [21] to guarantee a constant DC bus voltage and realize unity power factor in boost CHBML-AFE structure. However, SMC presents a couple of drawbacks, including problems with variable switching frequency and the occurrence of steady-state errors in the voltage output. The weak dynamic response of the SMC when a load transient occurs is due to the frequent sliding gain in the sliding surface function. This prevents the convergence of the tracking errors to zero in finite time. In order to mitigate the issue of constant sliding, the rotating sliding line was introduced in [22] to provide improvement to the dynamic response.

Voltage balancing is one of the main challenges in the implementation of CHBML-AFE topology. Voltage balancing control can be carried out either by a CHBML converter [3]– [5] or a CHBML converter and a DC-DC converter [6], [7]. Although, the first approach is more flexible, it has low time response because it uses PI controllers and the switching frequency of the CHBML converter is lower than that of the DC-DC converter. The second approach is expected to have better performance, however, the overall control system would be more complicated. Multiple methods have been studied in prior art to address output DC bus voltage balancing regulation. A PI-based control technique was proposed in [23] to correct the problem of unbalanced voltage of the CHBML-AFE by regulating the power circulation of the system. An indirect control method was utilized in [24] to guarantee that the DC link voltage was consistently balanced while keeping the AC current in phase with the grid voltage. In [25], a decoupled dq three-phase control strategy was studied to compensate for the unbalanced DC voltage and power of the converter. In [26], an adaptive grid current PR controller was analyzed to balance the DC voltage of the CHBML-AFE. In [27], a voltage-balancing technique based on the adaptive resonant algorithm used the estimated energy of the DC-link capacitor to monitor changes in the DC voltage of the converter.

In spite of the advantages of these control methods, there are drawbacks that cannot be ignored. Downsides to consider include undetermined current spectra, uncertainty under variable switching frequency, sensitivity to the system model accuracy, increased computational effort, and ineffectiveness under extremely distorted input voltage [26], [28]. Additionally, the global stability of the closed-loop system is not guaranteed, especially under a wide range of perturbations away from the operating point.

The LF based control method was successfully applied to regulate DC-DC converters [29], three-phase AC-DC converters [30], single-and three-phase shunt active power filters [31], [32], and grid-connected inverters [33]. Outstanding dynamic response and global stability under large signal transients are achieved through the use of the LF technique. A modified LF based control strategy for a single phase cascaded H-bridge multilevel inverter was proposed [34], and its performance was tested for nonlinear loads. Although the proposed controller provided low THD at the output voltage, this inverter had an LC filter at the output. Additionally, it required a derivative operator to generate inductor current reference.

Based on the excellent features of the LF based regulator method discussed in the above applications, this work presents an LF based current control method for the CHBML-AFE with LCL filter. The standard LF strategy is adjusted with an added capacitor voltage feedback loop, leading to inhibition of the LCL filter resonance. The converter side filter current and capacitor voltage feedback are used in the proposed expanded LF based control. In addition, the requirement of the second derivative and the dependency on filter components for generation of the converter side filter current reference are removed by using the PR control strategy. Thus, the steady-state error is eliminated. The proposed controllers are analysed and the transfer function of the system is obtained. Conditions for the gain values which ensure global asymptotic stability are also obtained. In addition to the suppression of the LCL filter resonance, the transient performance of the system is also improved with the proposed capacitor voltage feedback. The proposed control scheme utilizes a PI regulator for the DC voltage control. The use of an additional DC voltage balancing controller, which was introduced in [35] and [36], helps to prevent unbalanced DC voltage conditions. This proposed control system topology and its performance for both transient and steady-state conditions are verified in the simulation and experimental results.

The rest of the paper is structured as follows: The mathematical model of the CHBML-AFE is derived in Section II. The proposed LF based control scheme and PR based reference current generation is explained in Section III. Analysis and parameter determination process is covered in Section IV. In Section V, the results obtained from the simulation and experimental studies are discussed. Section VI presents the conclusions that are drawn.

II. Modelling of the CHBML-AFE

A single-phase CHBML-AFE is presented in Fig. 1. Three identical cascaded single-phase H-bridge cells form the converter structure. Three separate DC bus voltages, V_{o1}, V_{o2} and V_{o3}, are obtained. The reference value for any of the DC outputs is V_d. V_{H1}, V_{H2} and V_{H3} are the reflected output voltages, depending on the switching function (u). The H-bridge input terminals are connected in series to the utility grid, denoted as v_g, via the LCL filter. The LCL filter is

This work is licensed under a Creative Commons Attribution 4.0 License. For more information, see https://creativecommons.org/licenses/by/4.0/

This article has been accepted for publication in IEEE Open Journal of Power Electronics. This is the author's version which has not been fully edited and content may change prior to final publication. Citation information: DOI 10.1109/OJPEL.2023.3239414

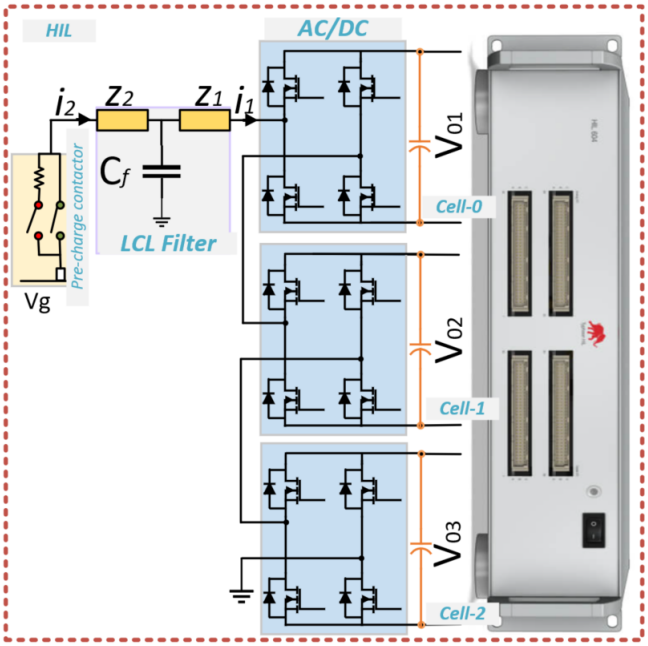


Fig. 1: The cascaded H-bridge active rectifier

comprised of the filter capacitor, C_f, and the impedances, Z_2 and Z_1, where L_2 and r_2 are the series combination of Z_2, and L_1 and r_1 are the series combination of Z_1. The voltage across C_f is denoted by V_{Cf}, where as i_{cf} is its current. The grid side and converter side currents are depicted with i_2 and i_1, respectively. The equations describing the CHBML-AFE can be written as (1) – (6).

$$\frac{L_2 di_2}{dt} + r_2 i_2 = v_g - v_{cf} \tag{1}$$

$$\frac{L_1 di_1}{dt} + r_1 i_1 = v_{cf} - (V_{H1} + V_{H2} + V_{H3}) \tag{2}$$

$$C_f \frac{dv_{cf}}{dt} = i_c = i_2 - i_1 \tag{3}$$

$$\begin{aligned} V_{H1} &= uV_{01} \\ V_{H2} &= uV_{02} \\ V_{H3} &= uV_{03} \end{aligned} \tag{4}$$

$$V_{01} = V_{02} = V_{03} = V_d \tag{5}$$

$$v_g = V_g sin(\omega t) \tag{6}$$

$$u = U_o + \Delta u \tag{7}$$

(7) represents the switching function (u) in which U_o and Δu are defined as the steady-state and unsettled values, respectively.

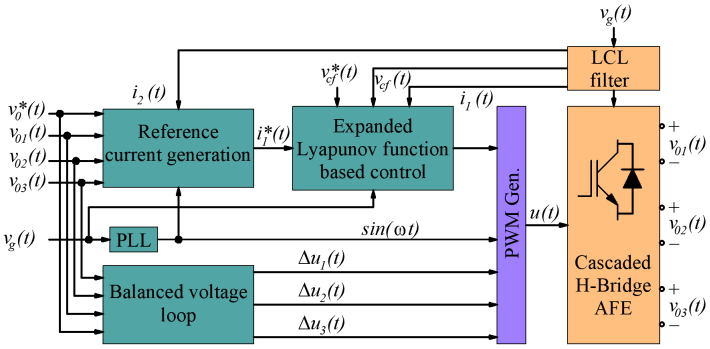


Fig. 2: The overall block diagram of the proposed strategy

III. The Control Scheme Based on LF and PR Control Methods

In this study, a novel control strategy is proposed for a CHBML-AFE converter. The proposed controller strategy is composed of a PI based output DC voltage control and cell output voltage balancing controller, a PR based reference current generation algorithm, and an expanded LF based current control scheme. The overall block diagram of the proposed strategy is shown in Fig. 2.

A. LF Based Current Control Scheme

To ensure the global stability of the CHBML-AFE converter around its equilibrium point of operation, the LF based controller has been utilized. The direct formulation of LF states that the state variables are at the equilibrium point when the supplied energy from the power source equals the total energy consumed by the load and AFE components. The state variables can be formulated in (8) - (10) where i_1^* , i_2^* and $V_{c_f}^*$ are the references for i_1, i_2 and V_{c_f}.

$$x_1 = i_1 - i_1^* \tag{8}$$

$$x_2 = i_2 - i_2^* \tag{9}$$

$$x_3 = v_{c_f} - v_{c_f}^* \tag{10}$$

From this stipulation, an energy based function can be developed to evaluate the stability of the system [36] - [38]. As formulated in Lyapunov's direct method, the equilibrium point is universally asymptotically stable if $V(x)$ meets the following criterion for all $x \neq 0$:

$$\begin{aligned} V(0) &= 0 \\ V(x) &> 0 \\ V(x) &\to \infty \\ \frac{dV}{dt} &> 0 \end{aligned} \tag{11}$$

The subsequent LF can be obtained from the stored energy in the inductors and capacitor:

$$V(x) = \Delta E_{L1} + \Delta E_{L2} + \Delta E_c = \frac{1}{2} L_1 x_1^2 + \frac{1}{2} L_2 x_2^2 + \frac{1}{2} C x_3^2 \tag{12}$$

This work is licensed under a Creative Commons Attribution 4.0 License. For more information, see https://creativecommons.org/licenses/by/4.0/

This article has been accepted for publication in IEEE Open Journal of Power Electronics. This is the author's version which has not been fully edited and content may change prior to final publication. Citation information: DOI 10.1109/OJPEL.2023.3239414

From (12) it can be concluded that $V(0) = 0$, $V(x) > 0$, for all $x \neq 0$ and $V(x) \to \infty$ as $||x|| \to \infty$. The time derivative of (12) is formulated to test the former statement and the global stability of the CHBML-AFE. The time derivative of the LF can be formulated as in (13):

$$\frac{dV(x)}{dt} = x_1 L_1 \frac{dx_1}{dt} + x_2 L_2 \frac{dx_2}{dt} + x_3 C_f \frac{dx_3}{dt} \tag{13}$$

By substituting equations (8) – (10) into (13), this equation can be rearranged, as below:

$$\frac{dV(x)}{dt} = -3V_d x_1 \Delta U - r_1 x_1^2 - r_2 x_2^2 \tag{14}$$

Here, $\frac{dV(x)}{dt} < 0$ if the disturbed input regulator is chosen as:

$$\Delta U = K_\alpha V_d x_1 \tag{15}$$

where $K_\alpha > 0$ and is a real constant. The ultimate formulation of the control input is presented in the following equation:

$$u = U_0 + \Delta U = \frac{1}{3V_d}\left(L_1^{'} \frac{di_1^*}{dt} + r_1^{'} i_1^* + {v_{cf}}^*\right) + K_\alpha V_d x_1 \tag{16}$$

where $L_1^{'}$, $L_2^{'}$, $r_1^{'}$, $r_2^{'}$ and $C_f^{'}$ represent the estimated values of the filter components L_1, L_2, r_1, r_2 and C_f, respectively. Multiplying the voltage regulator output and the unit sine wave, generated by the PLL to be synchronized to the grid voltage, produces the $i_2^*(t)$ function in (13) and (14). Once $i_2^*(t)$ is generated, ${v_{cf}}^*(t)$ and $i_1^*(t)$ are obtained, as in (17) and (18), respectively.

$${v_{cf}}^* = v_g - L_2^{'} \frac{di_2^*}{dt} - r_2^{'} i_2^* \tag{17}$$

$$i_1^* = i_2^* - i_c^* = i_2^* - C_f^{'} \frac{dv_g}{dt} + L_2^{'} C_f^{'} \frac{d^2 i_2^*}{dt} + r_2^{'} C_f^{'} \frac{di_2^*}{dt} \tag{18}$$

The control law in (16) yields a globally asymptotically stable operation. Yet, the damping produced is not effective in decreasing the oscillations which result from the complex conjugate poles of the LCL filter. In order to overcome this problem, the traditional LF based control law is adjusted with a capacitor voltage error x_3 feedback loop. This modification is presented in (19):

$$\Delta U = K_\alpha V_d x_1 - K_\beta x_3 \tag{19}$$

Substituting (19) into (14) gives:

$$\frac{dV(x)}{dt} = -3K_\alpha x_1^2 V_d^2 - r_1 x_1^2 - r_2 x_2^2 + 3K_\beta V_d x_1 x_3 \tag{20}$$

By considering the perfect match between the real and estimated values of the LCL filter components, the negative definiteness of $\frac{dV(x)}{dt}$ is ensured if the following inequality is met:

$$K_\beta < \left(K_\alpha V_d - \frac{r_1}{3V_d} - \frac{r_2 x_2^2}{3V_d x_1^2}\right)\frac{x_1}{x_3} \tag{21}$$

Thus, it is guaranteed that the proposed control law is globally asymptotically stable. Both the inverter current and the capacitor voltage feedback are included in the ultimate control law, as demonstrated below:

$$u = \frac{1}{3V_d}\left(L_1^{'} \frac{di_1^*}{dt} + r_1^{'} i_1^* + {v_{cf}}^*\right) + K_\alpha V_d x_1 - K_\beta x_3 \tag{22}$$

B. Reference Inverter Current Generation by Using PR Controller

Under disturbances away from the operating point, the closed-loop control is globally asymptotically stable using the formulation obtained in (22). However, obtaining i_1^* and ${v_{cf}}^*$ signals is crucial for the proposed control. Even though these signals can be obtained by using (17) and (18), generating i_1^* can be cumbersome and requires second order differentiation. Therefore, in this study, the PR control technique is used to generate the inverter reference current i_1^*. The dependency on the LCL filter parameters and the requirement for second order differentiation can be eliminated through the use of the PR regulator. It is well established that the PR regulator provides excellent tracking for AC signals along with an infinite gain at ω. As a result, the utility current will follow its reference without any error in steady-state operation. However, infinite gain is impossible in a practical system. Thus, in real world applications, the succeeding non-ideal transfer function equation given in (24) is utilized [39]. Eqs. (23) and (24) are the responses of the ideal and the non-ideal PR controller, respectively.

$$G_{pr}(s) = \frac{Y(s)}{E(s)} = K_p + \frac{2K_r s}{s^2 + \omega^2} \tag{23}$$

$$G_{pr}(s) = \frac{Y(s)}{E(s)} = K_p + \frac{2K_r \omega_c s}{s^2 + 2\omega_c s + \omega^2} \tag{24}$$

In (23) and (24), K_p is the proportional gain while K_r is the resonant gain. ω is the resonant frequency and ω_c is the cutoff frequency. The PR regulator output represents the inverter current reference and can be formulated using the Laplace domain, as in (25).

$$I_1^*(s) = [I_2^*(s) - I_2(s)]G_{pr}(s) \tag{25}$$

In addition, the use of (25) removes the requirement of the filter parameters, thus, improving the robustness of the

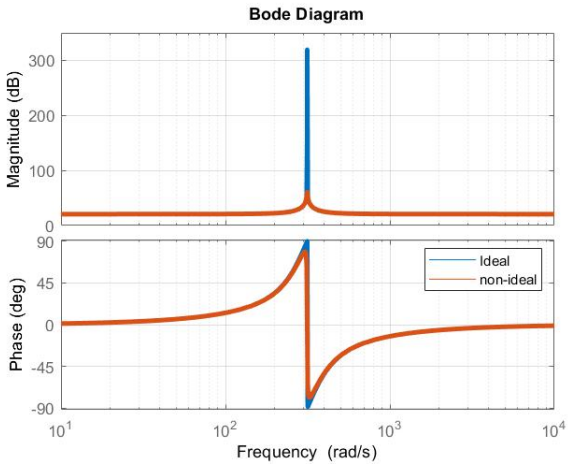


Fig. 3: The bode diagram of the ideal and non-ideal PR controller

This work is licensed under a Creative Commons Attribution 4.0 License. For more information, see https://creativecommons.org/licenses/by/4.0/

This article has been accepted for publication in IEEE Open Journal of Power Electronics. This is the author's version which has not been fully edited and content may change prior to final publication. Citation information: DOI 10.1109/OJPEL.2023.3239414

proposed controller. The magnitude and phase plots of the ideal versus the non-ideal PR regulators when $K_p = 10.83$, $K_r = 1080.33$, $\omega = 100\pi\frac{rad}{s}$, and $\omega_c = 1\frac{rad}{s}$ are shown in Fig. 3. It can be noted that the gain of the magnitude response of the non-ideal PR is significantly decreased, thus providing better performance.

IV. AFE Control Analysis

A. Analysis of the Grid Current Transfer Function

A closed-loop transfer function which links the reference current to the measured grid current is formulated in the frequency domain, as in (26), in order to predict the behavior of this system. To minimize the number of parameters and simplify the obtained transfer function, the filter inductor resistances r_1 and r_2 are omitted. Substituting the final switching control obtained in (22) into (2) gives rise to the following expression, as formulated in (26).

$$TF(s) = \frac{I_1(s)}{I_1^*(s)} = \frac{bs^3 + es^2 + gs + d\omega^2}{Ds^5 + Fs^4 + Gs^3 + Hs^2 + Ls + M} \tag{26}$$

where

$$\begin{aligned}
A &= L_1 + L_2(1 + 3K_\beta V_o) & a &= L_2^{'}(1 + 3K_\beta V_0) \\
B &= 2\omega_c L_1^{'}(K_p + K_r) & b &= a + L_1^{'}K_p \\
D &= C_f L_1 L_2 & d &= 3K_p K_\alpha V_o^2 \\
E &= 3K_\alpha V_o^2 C_f L_2 & e &= d + 2\omega_c(b + L_1^{'}K_r) \\
F &= E + 2D\omega_c & f &= 3K_r K_\alpha V_o^2 \\
G &= 2E\omega_c + A + D\omega^2 + L_1^{'}K_p & g &= b\omega^2 + 2\omega_c(d + f) \\
H &= 3K_\alpha V_o^2 + \omega^2 E + 2A\omega_c + B & I &= 6K_\alpha V_o^2 \omega_c + N \\
J &= 3K_\alpha V_o^2 \omega^2 & L &= I + d + f \\
M &= J + d\omega^2 & N &= (A + L_1^{'}K_p)\omega^2
\end{aligned}$$

It is seen from (26) that the presented control scheme is unaffected by changes in C_f. The characteristic equation can be used to analyze the stability of the closed system. Since $K_\alpha > 0$, $K_\beta > 0$, $K_p > 0$ and $K_r > 0$, it is inferred that the characteristic equation contains only positive constant coefficients. Application of the Routh–Hurwitz stability criterion leads to the following formulations given in (27) - (31):

$$FG - DH > 0 \tag{27}$$

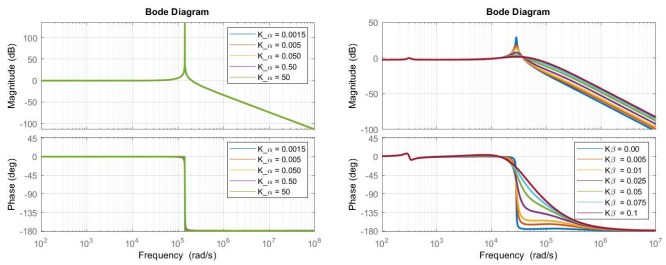
$$FL - DM > 0 \tag{28}$$

$$LF^2 - GFH - DMF + DH^2 > 0 \tag{29}$$

$$M > 0 \tag{30}$$

$$\begin{aligned} D^2M^2 - 2DFLM - DGHM + DH^2L \\ +F^2L^2 + FG^2M - FG > 0 \end{aligned} \tag{31}$$

The closed-loop system is stable when the above conditions (27) - (31) are satisfied. However, these conditions are not sufficient to determine the desired values of the controller. Determination of the control parameters will be explained in the next section.



(a) (b)

Fig. 4: The magnitude and phase responses (a) without the capacitor voltage feedback loop ($K_\beta = 0$) (b) with the capacitor voltage feedback loop ($K_\alpha = 0.05$ and $K_\beta \neq 0$)

B. Determination of Control Parameters

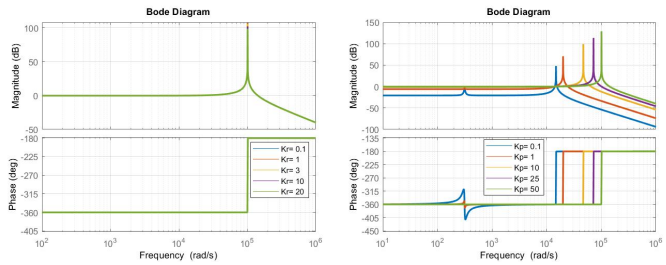
It can be seen from (26) that the transfer function and characteristic equation are fifth order. Thus, achievement of the optimum values of the controller gains analytically is cumbersome. Before focusing on the optimum parameter determination, effectiveness of the proposed voltage feedback loop was investigated. Fig. 4a and Fig. 4b show the frequency response of the proposed controller when there is a 10% deviation in all three component values of the LCL filter with and without the capacitor voltage feedback loop, respectively, at the same time. The gains of the PR controller are set to $K_p = 10.833$, $K_r = 1080.33$, $\omega = 120\pi\frac{rad}{s}$, and $\omega_c = 1rad/s$. It can be observed in Fig. 4a that although different K_α values were used in the control scheme, which does not contain the added capacitor voltage feedback loop ($K_\beta = 0$), the resonance cannot be damped. However, the desired resonance damping can be obtained when the added capacitor voltage loop is enabled, as depicted in Fig. 4b. The level of damping is related to the value of K_β. Additionally, when both control methods are used, it can be noted that there is no steady-state error (0 dB magnitude at 60 Hz) or phase shift (0^0 phase at 60 Hz) in the utility current. This provides evidence of the effectiveness of the PR regulator.

As mentioned above, the PR controller is used to obtain i_1^* from the utility current error $(i_2^* - i_2)$. It is worth noting that K_p influences the dynamics of the system, and K_r has an important role in decreasing steady-state error and dictating the bandwidth around the fundamental frequency [39], [40]. To determine the PR controller gains, K_α and K_β are fixed at $K_\alpha = 0.05$ and $K_\beta = 0.025$. The magnitude and phase responses of the PR controller for different K_p and K_r values are given in Fig. 5a and Fig. 5b. When K_r is increased, there is no change in the magnitude of the resonant peak. However, the bandwidth increases at 60 Hz. Since the gains of a PR regulator can be adjusted in the same manner as a PI regulator, the technical optimum criterion [40], [41] can be used to obtain K_p and K_r:

$$K_p = \frac{f_{sw}(L_1 + L_2)}{3} \tag{32}$$

This work is licensed under a Creative Commons Attribution 4.0 License. For more information, see https://creativecommons.org/licenses/by/4.0/

This article has been accepted for publication in IEEE Open Journal of Power Electronics. This is the author's version which has not been fully edited and content may change prior to final publication. Citation information: DOI 10.1109/OJPEL.2023.3239414



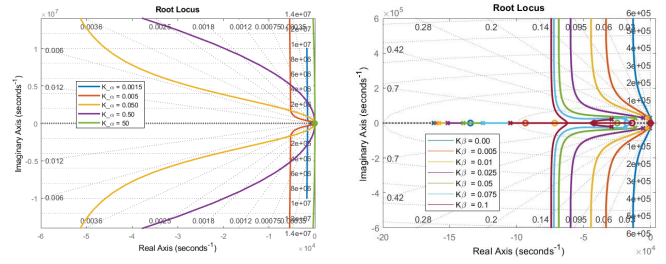
(a) (b)

Fig. 5: The magnitude and phase responses for (a) $K_r = 10$ (b) $K_p = 1200$

$$K_r = \frac{K_p(r_1 + r_2)}{L_1 + L_2} \tag{33}$$

The root locus graphs of the system for different K_α and K_β gains (with constant K_p and K_r) were obtained to observe the movement of the roots, and are given in Fig. 6a and Fig. 6b, respectively. As previously mentioned, the system is fifth order. However, the LF based controller mainly affects only three of the five poles (one complex conjugate pole pair and one real pole). The dynamic response of the system maintains global stability. The other complex conjugate pole pair is located near the imaginary axis in the s-plane and is only influenced by the gains of the PR regulator for the purpose of achieving a zero steady-state error in i_2.

Initially, K_β, K_p and K_r gains are kept constant. Fig. 6a represents the movement of the system poles when K_α varies. The movement of the real pole is not shown in Fig. 6a, as it is much larger than the real part of the complex conjugate poles. It is seen that the complex conjugate poles move away from the imaginary axis while the real pole (which is not seen in the figure) moves toward the imaginary axis. Additionally, K_α significantly affects the real part of the conjugate poles, but has comparatively less effect on the imaginary parts. Therefore, K_α improves the system dynamics but can provide limited resonance damping effect to suppress the oscillations introduced by the complex conjugate poles of the LCL filter. When K_β is increased from 0 to 0.1, as in Fig. 6b, the complex conjugate poles move away from the imaginary axis.



(a) (b)

Fig. 6: Root locus of the transfer function for different (a) K_α values (b) K_β values

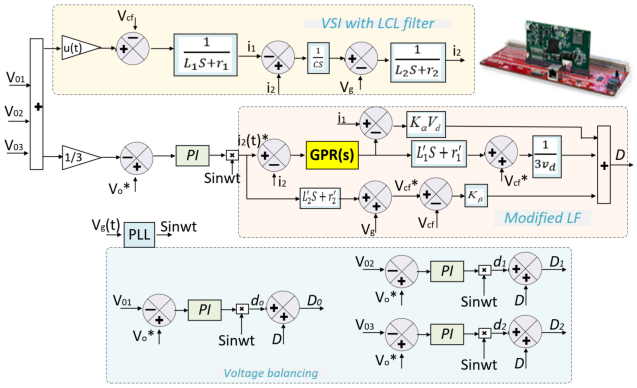


Fig. 7: Detailed block diagram of the proposed controller with capacitor feedback voltage loop and DC bus balancing.

The damping ratio increases while the real pole moves toward the imaginary axis. However, the damping ratio is decreased with larger K_β values, as the real pole moves toward zero. This leads to deterioration in the dynamic response and may risk the stability of the system. Therefore, optimum determination of the controller gains greatly affects the performance of the controller. Since the closed-loop transfer function is extremely complex, simulation studies are used to determine the K_α and K_β in order to obtain a fast dynamic response and globally stable system. In this study, controller gains are determined as $K_\alpha = 0.005$ and $K_\beta = 0.025$.

C. The Controller Structure

The proposed control scheme is given in Fig. 2, which shows the overall controller structure. Fig. 7 shows a detailed diagram of the controller. The overall control method contains three main parts: the generation of the grid current reference, the modified LF based current control method, and the output DC bus voltage balancing control. The grid reference current is obtained by summing the output voltages and then dividing that result by the number of DC buses present in the CHBML-AFE to obtain the average DC voltage value. This average voltage $(v_o(t))$ is subtracted from the reference DC output voltage value $(v_o^*(t))$ and the voltage error is obtained. By using this voltage error and the PI controller, the peak value of the current reference is obtained. By multiplying the output of the PI controller (peak value of the current reference) and the unit sine wave, which is synchronized with the grid voltage and frequency and generated by the PLL unit, the reference signal for the grid current is generated. This process is summarized in (34)

$$i_2^* = [K_p^{PI}(v_0^*(t) - v_0(t)) + K_i^{PI} \int (v_0^*(t) - v_0(t))\, dt] sin\omega t \tag{34}$$

where K_p^{PI} and K_i^{PI} are gains of the PI controller. This reference current is then fed to the PR controller block to produce the final reference for the modified LF. In addition to the LF based control with additional capacitor voltage loop and PR controller, a voltage balance controller is also applied to

This work is licensed under a Creative Commons Attribution 4.0 License. For more information, see https://creativecommons.org/licenses/by/4.0/

This article has been accepted for publication in IEEE Open Journal of Power Electronics. This is the author's version which has not been fully edited and content may change prior to final publication. Citation information: DOI 10.1109/OJPEL.2023.3239414

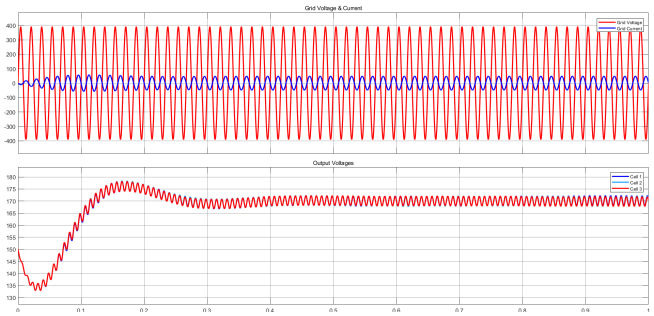
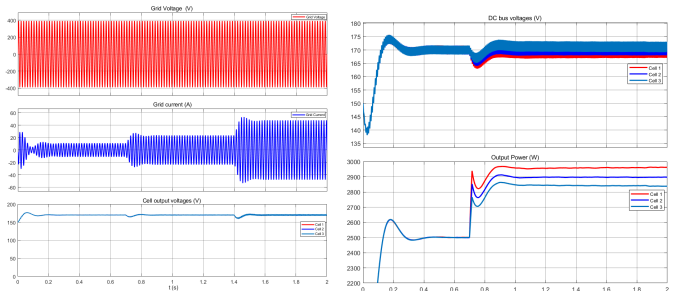


Fig. 8: Steady state performance of the AFE.



(a) (b)

Fig. 9: (a) Dynamic performance of the AFE (b) DC voltages and powers of the AFE under unbalanced condition.

balance the cell voltages of the CHBML-AFE. The goal of this voltage balance controller is to remove possible unbalanced voltage conditions for situations where mismatched parameters occur or different loads are applied to the cells of CHBML-AFE. The output DC voltage of each cell is controlled by another PI controller. The output of this second PI is then multiplied by the reference sine wave (the output of the PLL) to generate the perturbed duty cycles. These are added to the switching control, which is generated by the modified LF block. The relation between each block is seen in detail in Fig. 7.

V. Experimental and Simulation Results

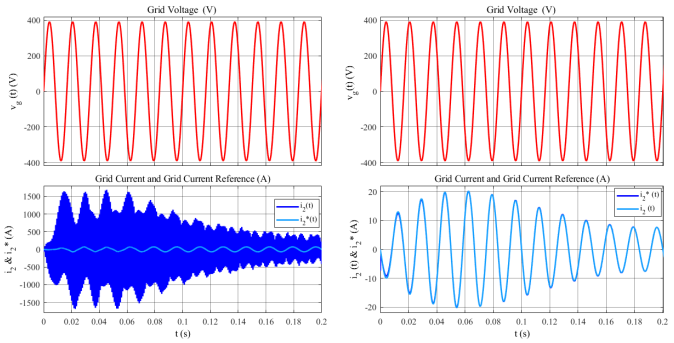
In this study, a single-phase three-cell CHBML-AFE was designed, simulated, and tested. Simulation results were obtained from the MATLAB/Simulink platform. The design parameters of the system are: $V_g = 277V$, $L_1 = 0.8mH$, $L_2 = 0.5mH$, $C_f = 10\mu F$, $r_1 = 0.08\Omega$, $r_2 = 0.05\Omega$ and $f_{sw} = 25kHz$. The design of the proposed configuration utilizes 277V grid voltage and generates 170V DC bus voltage per module.

A. AFE Simulation Results

Fig. 8 shows the grid voltage and current and the three DC bus voltages of the AFE. This figure demonstrates the performance of the AFE at steady state. It can be noticed that all three DC bus voltages are equal and the system exhibits low overshoot and low DC bus voltage ripple (2 volts). Additionally, the grid current is sinusoidal and in phase with the grid voltage.

The reference tracking performance of the DC bus voltages and grid current are also tested. The proposed system is run with three different loads levels. Both the transient response and steady-state performance of the proposed system are tested in three zones, as depicted in Fig. 9b. In Zone-1 (0s-0.7s), which is the low power region, the system runs with 23% load. In Zone-2 (0.7s-1.4s), the medium power region, a step load was applied to increase the load power to 50%. In the last case, a 50% load step up is added to test the system at full power (1.4s – 2s).

As seen in Fig. 9b, during load steps the control provides robust voltage and current tracking accuracy. It can be noticed that the system exhibits less than 10% undershoot. To further



(a) (b)

Fig. 10: Effect of K_β, (a) Without voltage loop ($K_\alpha = 0.005$ and $K_\beta = 0$), (b) Proposed approach with the voltage loop ($K_\alpha = 0.005$ and $K_\beta = 0.025$).

prove the performance of the control strategy, the THD of the grid current is measured for the low, medium, and high power regions. The THD levels of the current drawn from the grid are obtained as 3.05% for low power, 1.20% for medium power, and 0.85% for full power. The effect of the proposed additional capacitor voltage feedback loop is also investigated. As mentioned before, if the the oscillations introduced by the complex conjugate poles of the LCL filter are not damped, they may lead to instability. As can be seen from Fig. 10a, the conventional LF based control cannot guarantee the stability of the converter. By expanding the conventional LF based control with a proper capacitor voltage feedback, as is seen in Fig. 10b, the proposed control scheme can damp these oscillations and track the reference signals successfully.

To further validate the dynamic performance of the CHBML-AFE, unbalanced loading is applied at 0.7s. At the start, the converter is operating at steady-state under balanced conditions. A load step is applied to bring each cell of the converter to a different power level, as shown in Fig. 9b. It is seen that during the unbalanced operation, the converter maintains high DC voltage tracking accuracy (with a 1.2 volt difference between the DC bus voltages) and draws sinusoidal current which is in phase with the grid voltage.

This work is licensed under a Creative Commons Attribution 4.0 License. For more information, see https://creativecommons.org/licenses/by/4.0/

This article has been accepted for publication in IEEE Open Journal of Power Electronics. This is the author's version which has not been fully edited and content may change prior to final publication. Citation information: DOI 10.1109/OJPEL.2023.3239414

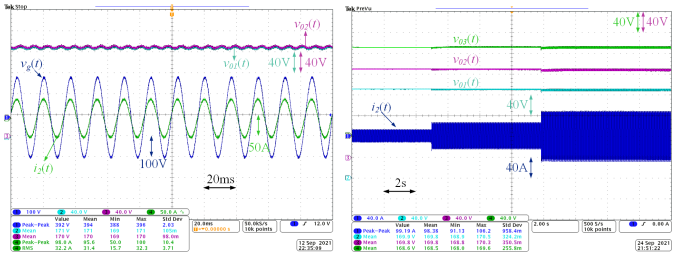
B. HIL Setup for The AFE

In order to validate the proposed controller for the CHBML-AFE, the Typhoon HIL 604 device is used to model the power stage, as seen in Fig. 1. The grid, the passive components, and the power MOSFETs are modeled using the Typhoon library. HIL is a closed-loop, model-based computerized testing solution and runs the model in real time. In this HIL testing, the controller under test (the derived modified LF based controller) is designed using the MATLAB/Simulink autocode generation capability. The generated code is uploaded to the TMDSCNCD28388D control card, as seen in Fig. 7. This control card is connected to the Typhoon hardware through the Typhoon HIL interface board (HIL DSP 180 Interface), and thus the communication between the control and the power stage can be established. The Typhoon HIL interface board is directly connected to a real-time HIL 604 simulator. This configuration facilitates HIL testing to establish how the actual controller will perform with the physical system at higher precision than would be possible in a fully simulated laboratory environment.

Fig. 11a - Fig. 14a demonstrate the results of the HIL experimental study of the AFE converter.

Fig. 11a shows the grid current and voltage, and two of the three DC bus voltages of the experimental results when the converter is operating at steady-state. Fig. 11b illustrates the dynamic performance of the converter. Here, the three DC bus voltages and the grid current are shown. Similar to the simulation, the three operating regions of the converter are tested to validate both the steady-state and transient performance of the controller. It can be seen from the figure that the grid current presents smooth transient with no oscillations. The undershoots observed in the DC bus voltages during transients are less than the 10% over/undershoot design specification. Fig. 12a shows the performance of the converter for abrupt load changes. During these tests, the proposed robust grid current control method and the output voltage regulation technique are proved to be effective in maintaining the proper operation of the converter. As demonstrated in these figures, the CHBML-AFE with the proposed control strategy generates balanced cell voltages and draws sinusoidal current from the grid. The harmonics content of the current signal is low and the THD value is measured as 2.7%.

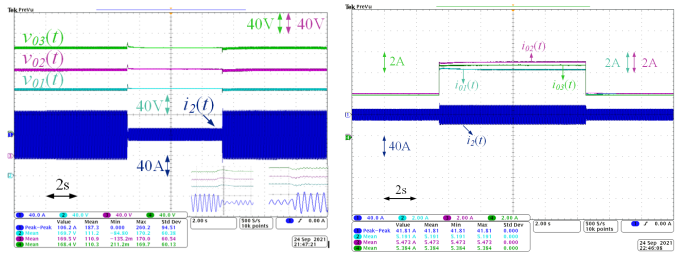
Fig. 12b - Fig. 13b show the performance of the proposed control schemes for both balanced and unbalanced load conditions. Fig. 12b shows the three output DC currents and the grid current for a light load unbalance. Fig. 13a shows the three output DC currents and the grid current and Fig. 13b shows the three DC bus voltages and the grid current for a heavy load unbalance. In this scenario, the system was initially operating under balanced conditions. A load step up is applied to bring the converter to unbalanced operation, which can be seen in the different levels of the DC output currents. During the unbalanced stage, each cell of the converter is operating under a different power level. The load level is changed again to bring the converter back to normal operation. This test is



(a) (b)

Fig. 11: (a) Grid voltage and current, and the DC bus voltages (b) Grid current and DC voltage waveforms when step load changes are applied ($K_\alpha = 0.005$ and $K_\beta = 0.025$)

.



(a) (b)

Fig. 12: (a) Worst case of load steps (b) Output DC currents and grid current during both balanced and unbalanced operation ($K_\alpha = 0.005$ and $K_\beta = 0.025$)

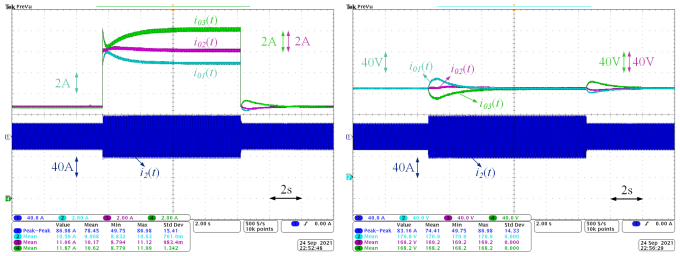
.

designed to specifically check the DC voltage control. It is seen that the output voltages maintained stable and balanced. In both step up and step down load tests, the converter maintained good transient and steady-state performance with minimal disturbance. Based on these results, it can be concluded that the proposed control strategy utilizing the voltage balancing control and the LF based current control supported with the additional capacitor feedback loop and PR controller provide excellent steady-state and transient response with very limited overshoot and undershoot. Additionally, all the output voltages are well balanced, even during unbalanced load conditions.

The effect of varying the K_β and K_α parameters to determine the optimal range of operation for these parameters is also investigated. As presented in the root locus analysis, K_α gains significantly affect the real part of the conjugate poles, but have comparatively less effect on the imaginary parts. Therefore, K_α improves the system dynamics by reducing the overshoot and undershoot during load steps, but can provide limited resonance damping effect to suppress the oscillations introduced by the complex conjugate poles of the LCL filter. When K_α is increased to a larger number, the oscillations worsen and will potentially lead the system to unstable operation. Fig. 14a demonstrates the effect of increasing the value of K_α up to its upper limit before the system becomes unstable. The increased oscillations on the grid current and resultant slower response of the DC output voltage can be easily seen

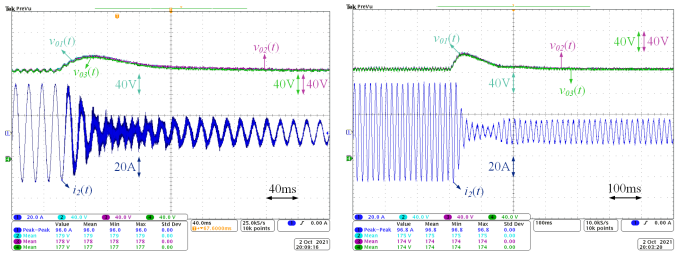
This work is licensed under a Creative Commons Attribution 4.0 License. For more information, see https://creativecommons.org/licenses/by/4.0/

This article has been accepted for publication in IEEE Open Journal of Power Electronics. This is the author's version which has not been fully edited and content may change prior to final publication. Citation information: DOI 10.1109/OJPEL.2023.3239414



(a) (b)

Fig. 13: (a) Output DC currents and grid current during both balanced and unbalanced operation (b) Output DC voltages and grid current during both balanced and unbalanced operation ($K_\alpha = 0.005$ and $K_\beta = 0.025$)



(a) (b)

Fig. 14: Zoomed DC bus voltages and grid current for large gain values (a) $K_\alpha = 300$ and $K_\beta = 0.025$, (b) ($K_\alpha = 0.005$ and $K_\beta = 30$.

from the figure.

When K_β is chosen within the range determined in Section V from the root locus plot, the damping ratio increases. As can be seen from the root locus plot, while K_β is increasing, the real pole moves toward the imaginary axis and the complex conjugate poles, which are originally close to the imaginary axis, move away from the imaginary axis. Thus, the damping effect of the controller improves. However, the damping ratio is decreased with larger K_β values, as the real pole moves toward zero. This may lead to deterioration in the dynamic response, higher overshoot and undershoot, and may risk the stability of the system. However, it should be noticed that even for a large value of K_β, the oscillations are considerably decreased compared to the large value of K_α. This definitively demonstrates the significance of the added capacitor voltage loop for providing better damping and reduction of oscillations. Fig. 14b demonstrates the effect of increasing the value of K_β. It can be seen that large K_β value deteriorate the dynamic performance of the controller. Therefore, optimum determination of the controller gains greatly affects the performance of the controller. Since the closed-loop transfer function is extremely complex, simulation and experimental studies are used to determine the optimal range for K_β and K_α in order to obtain a fast dynamic response and globally stable system.

The performance of the converter without the added capacitor voltage feedback loop is also investigated and is given in Fig.15. When $K_\beta \approx 0$, a similar scenario as presented in Fig. 12a is reproduced to compare the effect of the proposed additional capacitor voltage loop on the converter. The difference between Fig. 12a and Fig. 15 clearly shows how the added capacitor voltage loop improves the dynamic response of the converter. As presented in the control analysis section, removing the additional capacitor voltage feedback loop introduces larger overshoot and undershoot, creates more oscillations, and increases the settling time.

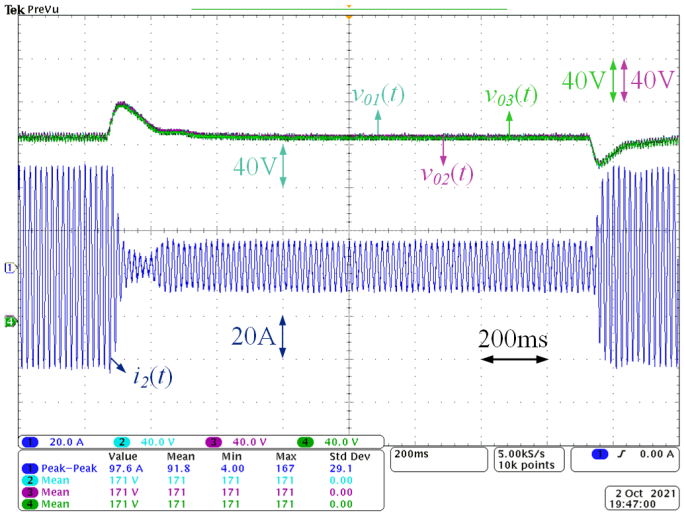


Fig. 15: DC bus voltages and grid current when ($K_\alpha = 0.005$ and $K_\beta \approx 0$.

A comparison of methods from past literature has been performed and is presented in Table I. Due to the limited number of studies on the CHB-AFE rectifier with LCL filter, studies on the grid-connected CHB inverter with LCL filter are also considered. As can be seen from the table, the proposed method provides better performance than the other control methods in terms of robustness, grid current THD, dynamic response, and steady-state error, while ensuring global stability. Additionally, the proposed control scheme also offers DC bus voltage balancing.

TABLE I: Comparison of four control approaches (Proposed method = PM, Guaranteed = Gd, Not reported = NR, Depends on filter parameters = DFP, Not needed = NN, Eliminated = El).

Comparison category	**Methods**			
	[42]	**[43]**	**[44]**	**PM**
THD (%)	NR	$\leq 5\%$	NR	2.7%
Global stability	Gd	NR	Gd	Gd
Robustness	DFP	DFP	Very good	Very good
Stead-state error	El	El	NR	El
Damping resistor	NN	NN	NN	NN
Dynamic response	Fast	Fast	Fast	Very fast
DC bus voltage balancing	NR	NR	No	Yes

This work is licensed under a Creative Commons Attribution 4.0 License. For more information, see https://creativecommons.org/licenses/by/4.0/

This article has been accepted for publication in IEEE Open Journal of Power Electronics. This is the author's version which has not been fully edited and content may change prior to final publication. Citation information: DOI 10.1109/OJPEL.2023.3239414

VI. Conclusion

In this study, a control strategy is proposed for a single-phase three-cell CHBML-AFE with LCL filter. The proposed control strategy employs a modified LF based current control, a PI based voltage control, and a cell voltage balancing control. The PI based voltage controller is used for the DC voltage control. It also generates the amplitude of the current reference signal. An additional capacitor voltage feedback loop is used to modify the conventional LF based current control method in order to suppress the resonance introduced by the LCL filter. The AFE current reference signal is generated by the designed PR controller to decrease dependency on the system parameters and improve the robustness of the system. The DC voltage balancing control is also applied to keep the output voltage balanced, even when the load is unbalanced. Analysis of the grid current transfer function, the influence of the PR control gains, and the expanded LF based control parameters have been studied to determine the performance of the employed control strategy. The simulation and experimental results prove that the proposed control strategy provides fast transient response, eliminates steady-state error, and keeps the cell voltages equal in both balanced and unbalanced load conditions. Additionally, it is seen that the resonance effect of the LCL filter is successfully suppressed, the current drawn from the grid is sinusoidal, and the THD level is measured as 2.7%.

Acknowledgment

This material is based upon work supported by the National Science Foundation under Grant No. 1650470. Any opinions, findings, and conclusions or recommendations expressed in this material are those of the author(s) and do not necessarily reflect the views of the National Science Foundation. Dr. Necmi Altin thanks financial support from the Scientific and Technological Research Council of Turkey (TUBİTAK) BIDEB-2219 Postdoctoral Research Program.

References

[1] J. Wen and K. Ma Smedley, "Synthesis of Multilevel Converters Based on Single- and/or Three-Phase Converter Building Blocks," IEEE Trans. Power Electron., vol. 23, no. 3, pp. 1247-1256, May 2008.

[2] N. B. Kadandani, S. Ethni, M. Dahidah and H. Khalfalla, "Modelling, Design and Control of Cascaded H-Bridge Single Phase Rectifier,"2019 10th International Renewable Energy Congress (IREC), Sousse, Tunisia, 2019, pp. 1-6.

[3] C. Qi, X. Chen, L. Su and Z. Lang, "Two-voltage hierarchical model predictive control for a single-phase cascaded H-bridge rectifier," IET Power Electronics, vol. 12, no. 7, pp. 1634-1642, 2019.

[4] Z. Yang, J. Sun, X. Zha and Y. Tang, "Power Decoupling Control for Capacitance Reduction in Cascaded-H-Bridge-Converter-Based Regenerative Motor Drive Systems," IEEE Transactions on Power Electronics, vol. 34, no. 1, pp. 538-549, Jan. 2019.

[5] R. Pena-Alzola, M. Liserre, F. Blaabjerg, R. Sebastion, J. Dannehl, and F. W. Fuchs, "Analysis of the passive damping losses in LCL-filter-based grid converters," IEEE Trans. Power Electron., vol. 28, no. 6, pp. 2642–2646, Jun. 2013.

[6] D. Pan, X. Ruan, C. Bao, W. Li, and X. Wang, "Capacitor-currentfeedback active damping with reduced computation delay for improving robustness of LCL-type grid-connected inverter," IEEE Trans. Power Electron., vol. 29, no. 7, pp. 3414–3427, Jul. 2014.

[7] J. Xu, S. Xie, and T. Tang, "Active damping-based control for grid-connected LCL-filtered inverter with injected grid current only," IEEE Trans. Ind. Electron., vol. 61, no. 9, pp. 4746–4758, Sep. 2014.

[8] A. Reznik, M. G. Simoes, A. Al-Durra and S. M. Muyeen, " LCL filter design and performance analysis for grid-interconnected systems ", IEEE Trans. Ind. Appl., vol. 50, no. 2, pp. 1225-1232, Mar./Apr. 2014.

[9] A. Kawamura, R. Chuarayaratip, and T. Haneyoshi, "Deadbeat control of PWM inverter with modified pulse patterns for uninterruptible power supply," IEEE Trans. Ind. Electron., vol. 35, no. 2, pp. 295–300, May 1988.

[10] C. Hua, "Two-level switching pattern deadbeat DSP controlled PWM inverter," IEEE Trans. Power Electron., vol. 10, no. 3, pp. 310–317, May 1995.

[11] C. Qi, X. Chen, P. Tu and P. Wang, "Cell-by-Cell-Based Finite-Control-Set Model Predictive Control for a Single-Phase Cascaded H-Bridge Rectifier," IEEE Transactions on Power Electronics, vol. 33, no. 2, pp. 1654-1665, Feb. 2018.

[12] C. Cecati, A. Dell'Aquila, M. Liserre and V. G. Monopoli, "Design of H-bridge multilevel active rectifier for traction systems," IEEE Transactions on Industry Applications, vol. 39, no. 5, pp. 1541-1550, Sept.-Oct. 2003.

[13] B.-R. Lin and H.-H. Lu, "New multilevel rectifier based on series connection of H-bridge cell," IEE Proceedings - Electric Power Applications, vol. 147, no. 4, pp. 304-312, July 2000.

[14] H. Iman-Eini, J. Schanen, S. Farhangi and J. Roudet, "A Modular Strategy for Control and Voltage Balancing of Cascaded H-Bridge Rectifiers," IEEE Trans. Power Electron., vol. 23, no. 5, pp. 2428-2442, Sept. 2008.

[15] A. Kuperman, "Proportional-Resonant Current Controllers Design Based on Desired Transient Performance," IEEE Trans. Power Electron., vol. 30, no. 10, pp. 5341-5345, Oct. 2015.

[16] P. Zanchetta, D. B. Gerry, V. G. Monopoli, J. C. Clare, and P. W. Wheeler, "Predictive Current Control for Multilevel Active Rectifiers with Reduced Switching Frequency," IEEE Trans. Ind. Electron., vol. 55, no. 1, pp. 163-172, Jan. 2008.

[17] P. Karamanakos, K. Pavlou and S. Manias, "An Enumeration-Based Model Predictive Control Strategy for the Cascaded H-Bridge Multilevel Rectifier," IEEE Trans. Ind. Electron., vol. 61, no. 7, pp. 3480-3489, July 2014.

[18] A. Moeini, H. Zhao and S. Wang, "A Current-Reference-Based selective harmonic current mitigation PWM technique to improve the performance of cascaded H-Bridge multilevel active rectifiers," IEEE Trans. Ind. Electron., vol. 65, no. 1, pp. 727-737, Jan. 2018.

[19] M. Carpita and M. Marchesoni, "Experimental study of a power conditioning system using sliding mode control," IEEE Trans. Power Electron., vol. 11, no. 4, pp. 731–742, Sep. 1996.

[20] L. Malesani ,L. Rosetto, G. Spiazzi, and A. Zuccato,"An ac power supply with sliding-mode control," IEEE Ind. Appl. Mag.,vol.2, no.5, pp.32–38, Sep./Oct. 1996.

[21] A. X. Kaletsanos, I. S. Manolas, K. G. Pavlou and S. N. Manias, "Sliding mode control for cascaded H-bridge boost rectifiers," 2010 IEEE International Symposium on Industrial Electronics, Bari, 2010, pp. 1070-1075.

[22] H. Komurcugil, "Rotating-sliding-line-based sliding-mode control for single-phase UPS inverters," IEEE Trans. Ind. Electron., vol. 59, no. 10, pp. 3719–3726, Oct. 2012.

[23] Tao, Xing-Hua, Yong-Dong Li, and Min Sun. "A PI-Based Control Scheme for Primary Cascaded H-Bridge Rectifier in Transformerless Traction Converters" Journal of International Conference on Electrical Machines and Systems, 1, no. 3 (January 2012): 360–65.

[24] Marzoughi, A., and H. Iman-Eini. "Indirect Control for Cascaded H-Bridge Rectifiers with Unequal Loads.", 2012 3rd Power Electronics and Drive Systems Technology (PEDSTC), 2012.

[25] Wang, Liang, Donglai Zhang, Yi Wang, Bin Wu, and Hussain S. Athab. "Power and Voltage Balance Control of a Novel Three-Phase Solid-State Transformer Using Multilevel Cascaded H-Bridge Inverters for Microgrid Applications." IEEE Trans. Power Electron., 31, no. 4 (2016): 3289–3301.

[26] Sha, Deshang, Guo Xu, and Yaxiong Xu. "Utility Direct Interfaced Charger/Discharger Employing Unified Voltage Balance Control for Cascaded H-Bridge Units and Decentralized Control for CF-DAB Modules." IEEE Trans. Ind. Electron., 64, no. 10 (2017): 7831–41.

[27] Blahnik, Vojtech, Tomas Kosan, Zdenek Peroutka, and Jakub Talla. "Control of a Single-Phase Cascaded H-Bridge Active Rectifier Under

This work is licensed under a Creative Commons Attribution 4.0 License. For more information, see https://creativecommons.org/licenses/by/4.0/

This article has been accepted for publication in IEEE Open Journal of Power Electronics. This is the author's version which has not been fully edited and content may change prior to final publication. Citation information: DOI 10.1109/OJPEL.2023.3239414

Unbalanced Load." IEEE Trans. Power Electron., 33, no. 6 (2018): 5519–27.

[28] Y. Su, X. Ge, D. Xie and K. Wang, "An Active Disturbance Rejection Control-Based Voltage Control Strategy of Single-Phase Cascaded H-Bridge Rectifiers," in IEEE Transactions on Industry Applications, vol. 56, no. 5, pp. 5182-5193, Sept.-Oct. 2020, doi: 10.1109/TIA.2020.3004316.

[29] S. R. Sanders and G. C. Verghese, "Lyapunov-based control for switched power converters", IEEE Trans. Power Electron., vol. 7, no. 1, pp. 17–24, Jan. 1992.

[30] H. Komurcugil and O. Kukrer, "Lyapunov-based control for three-phase PWM AC/DC voltage-source converters," IEEE Trans. Power Electron., vol. 13, no. 5, pp. 801–813, Sep. 1998.

[31] H. Komurcugil and O. Kukrer, "A new control strategy for single-phase shunt active power filters using a lyapunov function," IEEE Trans. Ind. Electron., vol. 53, no. 1, pp. 305–312, Feb. 2006.

[32] Rahmani, A. Hamadi, and K. Al-Haddad, "A Lyapunov-function-based control for a three-phase shunt hybrid active filter," IEEE Trans. Ind. Electron., vol. 59, no. 3, pp. 1418-1429, March 2012.

[33] C. Meza, D. Biel, D. Jeltsema, and J. M. A. Scherpen, "Lyapunov based control scheme for single-phase grid-connected PV central inverters," IEEE Trans. Control Syst. Technol., vol. 20, no. 2, pp. 520–529, Mar. 2012.

[34] K. Biju and R. Ramchand, "A Modified Lyapunov Function Based Control Strategy for Single Phase Cascaded H-bridge Multilevel Inverter with Nonlinear Loads," 2019 IEEE Industry Applications Society Annual Meeting, 2019, pp. 1-6, doi: 10.1109/IAS.2019.8912341.

[35] H. Li, Y. Wang and C. Yu, "Research on voltage balance and power balance control for three-phase cascaded multilevel converter based power electronic transformer," IECON 2016 - 42nd Annual Conference of the IEEE Industrial Electronics Society, Florence, 2016, pp. 3588-3593.

[36] G. Jean-Pierre, N. Altin, A. E. Shafei and A. Nasiri, "A Control Scheme Based on Lyapunov Function for Cascaded H-Bridge Multilevel Active Rectifiers," 2020 IEEE Applied Power Electronics Conference and Exposition (APEC), New Orleans, LA, USA, 2020, pp. 2021-2026.

[37] H. Komurcugil, N. Altin, S. Ozdemir, and I. Sefa, "An extended Lyapunov-function-based control strategy for single-phase UPS inverters," IEEE Trans. Power Electron., vol. 30, no. 7, pp. 3976-3983, July 2015.

[38] I. Sefa, S. Ozdemir, H. Komurcugil, and N. Altin, "Comparative study on lyapunov-function-based control schemes for single-phase grid-connected voltage-source inverter with LCL filter," IET Renew. Power Gen., vol. 11, no. 11, pp. 1473–1482, 2017.

[39] R. Teodorescu, F. Blaabjerg, M. Liserre, and P. Loh, "Proportional resonant controllers and filters for grid-connected voltage-source converters," Proc. Inst. Electr. Eng.—Electr. Power Appl., vol. 153, no. 5, pp. 750–762, Sep. 2006.

[40] H. Komurcugil, N. Altin, S. Ozdemir, I. Sefa,"Lyapunov-Function and Proportional-Resonant-Based Control Strategy for Single-Phase Grid-Connected VSI With LCL Filter", IEEE Trans. Power Electron., Vol. 63, No. 5, pp. 2838-2849, May 2016

[41] R. Pena-Alzola, M. Liserre, F. Blaabjerg, M. Ordonez, and Y. Yang, "LCL-filter design for robust active damping in grid connected converters," IEEE Trans. Ind. Informat., vol. 10, no. 4, pp. 2192–2203, Nov. 2014.

[42] Y. Han, H. Chen, Z. Li, P. Yang, L. Xu and J. M. Guerrero, "Stability Analysis for the Grid-Connected Single-Phase Asymmetrical Cascaded Multilevel Inverter With SRF-PI Current Control Under Weak Grid Conditions," in IEEE Transactions on Power Electronics, vol. 34, no. 3, pp. 2052-2069, March 2019.

[43] H. Katir et al., "Fault Tolerant Backstepping Control for Double-Stage Grid-Connected Photovoltaic Systems Using Cascaded H-Bridge Multilevel Inverters," in IEEE Control Systems Letters, vol. 6, pp. 1406-1411, 2022.

[44] G. Jean-Pierre, N. Altin and A. Nasiri, "Sliding Mode Control Scheme of a Cascaded H-Bridge Multilevel Active Front End Rectifier," 2021 IEEE 12th International Symposium on Power Electronics for Distributed Generation Systems (PEDG), 2021, pp. 1-6.

This work is licensed under a Creative Commons Attribution 4.0 License. For more information, see https://creativecommons.org/licenses/by/4.0/